Solvation Dynamics and Evolution of the Spatial Extent of Photoinjected Electrons in D_2O/Cu(111)

Uwe Bovensiepen,* Cornelius Gahl, and Martin Wolf

Freie Universität Berlin, Fachbereich Physik, Arnimallee 14, 14195 Berlin-Dahlem, Germany

Received: March 13, 2003; In Final Form: April 25, 2003

Time- and angle-resolved two-photon-photoelectron (2PPE) spectroscopy is used to investigate the femtosecond dynamics of electron localization and solvation in ultrathin ice layers adsorbed on a Cu(111) single-crystal surface. An ultrashort UV pump pulse excites electrons in the Cu substrate to electronic states above the Fermi level (E_F), whereby wave function overlap with the conduction band of the ice mediates electron transfer into the adlayer. Apart from relaxation back to the metal substrate, the conduction band electrons in the ice layer localize within the first 50 fs in an electronic state at 2.9 eV above E_F. The localization process is revealed by a pronounced temporal change in the dispersion of the binding energy with electron momentum, $\hbar k_{||}$. Subsequently, molecular reorientation stabilizes this localized electron on a picosecond time scale as observed by an increase of the binding energy with 270 meV/ps. Considering the absence of a temperature dependence in the spectra between 25 and 100 K, we exclude hopping processes of the localized electron between sites of different binding energy. We rather attribute the stabilization to electron solvation, in accordance with the line shape and the temporal evolution of the localized electronic state. By exploiting the angular dependence of the 2PPE spectra, we can separate the conduction band and the solvated, localized state in ice, which allows us to determine the position of the conduction band minimum to be 2.9 eV above E_F. While the delocalized electrons in the conduction band exhibit a positive dispersion, the characteristic feature of the solvated state is an apparently negative dispersion at all time delays. As shown by model calculations of the electron momentum distribution as a function of binding energy, this observation is consistent with a solvated, localized electron with an increasing spatial confinement of its wave function evolving in parallel to electron solvation (i.e., increasing binding energy). From the width of the $k_{||}$ distribution an energy-dependent spatial extent of the probability density of the solvated electron is found which changes within 1.3 ps from about 20 Å to 10 Å. This finding thus corroborates the correlation of energetic stabilization and spatial extent of the electronic wave function during the process of electron solvation. On the basis of a simple model potential for a localized electron, we discuss the perturbation of the final state wave function and its influence on the analysis of angle-resolved photoemission spectra.

Introduction

An excess electron in a polar liquid like water can be stabilized by a rearrangement of the molecular environment. Thus, the binding energy of such an electron, which is commonly referred to as a solvated (or hydrated) electron, is larger than its quasi-free counterpart residing in the conduction band (CB).[1,2] Solvation of an initially delocalized electron originates from screening of the excess electron density leading to localization of the electronic wave function. The hydrated electron in liquid water may be regarded as a prototype system and has always attracted special interest. However, despite several decades of intense research, even basic properties such as the absorption spectrum or the microscopic structure are not fully understood. Due to the ultrafast molecular relaxation time below 1 ps, only the advent of femtosecond laser pulses enabled experimentalists to resolve the ultrafast dynamics of the generation of hydrated electrons in liquid water. While this process has been studied extensively by experiment[3−7] as well as theory,[1,8−10] some controversial issues remain. For example, Laenen et al. reported energetic relaxation of the hydrated electron through a sequence of precursor and excited states preceding the equilibrated state.[7] In contrast to that, Hertwig et al. proposed recently that ground-state dynamics dominate the relaxation of the solvated electron.[11]

Considering photoinduced electron injection into continuum states of water, the process of electron solvation involves not only energetic relaxation but also localization and increasing constriction of the electronic wave function. In principle, an experimental determination of the energetic stabilization and the spatial extent of the potential well would yield complementary information, which might serve as an input for theoretical descriptions. The calculated electron−oxygen radial distribution for the equilibrated hydrated electron predicts a spatial extent of the first solvation shell of 4−5 Å in diameter,[9] which is in accordance with the smallest water cluster of five molecules that sustains electron solvation.[12] The diameter of the first solvation shell was also derived for aqueous glasses from electron spin−echo measurements,[13] and the result is identical with the above calculation for the liquid phase. In a three-pulse experiment Barbara and co-workers determined the spatial extent of excited states indirectly by evaluating the geminate recombination dynamics of a solvated electron−hole pair.[14−16] These authors report that the s-state is localized within <6 Å diameter,

* Corresponding author. Telephone: +49 30 838 53340. Fax: +49 30 838 56059. E-mail: uwe.bovensiepen@physik.fu-berlin.de.

10.1021/jp034654g CCC: $25.00
Published on Web 07/18/2003

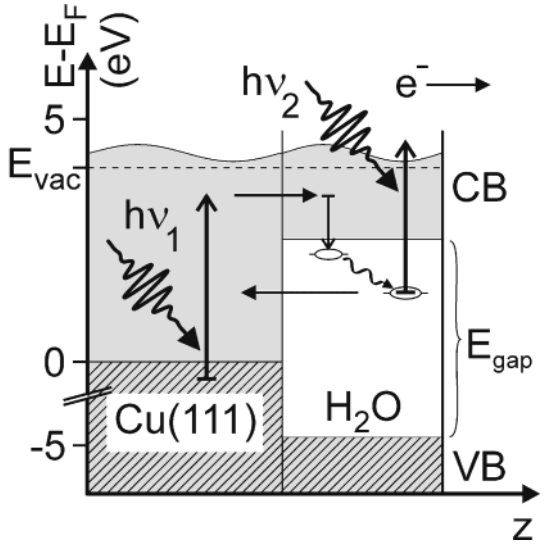

Figure 1. Schematic diagram of the 2PPE experiment and the electronic structure of the ice layer on Cu(111), which illustrates the elementary steps of the electronic process at the Cu−ice interface by arrows: optical excitation in Cu; electron transfer into the ice CB; localization and solvation of the electron followed by back transfer to the metal.

and that the conduction band states of the solvated electron extend over more than 60 Å. However, a direct measurement is not available.

In this work, we follow a conceptually different approach to electron solvation. We study localization and solvation dynamics of electrons injected into an ultrathin ice layer grown in situ on a Cu(111) single crystal surface in ultrahigh vacuum (UHV). Thus, our study focuses on electron solvation dynamics in atomically thin ice layers near a metal interface rather than on bulk ice. Such a surface science approach to the problem enables the investigation of structural aspects of electron solvation dynamics since the structure of ice layers can be altered on purpose, for example by varying coverage, growth parameters, and the substrate, which serves as a template for the ice layer. Such structural aspects are discussed elsewhere.[21] We employ time-resolved two-photon-photoelectron spectroscopy (2PPE). In contrast to optical spectroscopy, which is usually used to study the electron solvation dynamics, 2PPE allows measurement of absolutely binding energy and electron momentum parallel to the surface $\hbar k_{||}$. The Cu substrate is employed as a source of electrons, which are photoinjected into the ice layer. In this way, photoionization of H_2O is not required to create quasi-free electrons. As this is a rather complicated process on its own, it might create intermediate states which possibly mask spectral features of the solvated electron.[7] In the past decade, 2PPE has shown to be a powerful tool to study the ultrafast electron dynamics at surfaces and interfaces. For example, a very detailed understanding was achieved for image potential states of bare metal surfaces[17,18] and metal surfaces covered with molecular overlayers.[19,20] Since the method is very sensitive to structural changes, special emphasis has to be put onto sample characterization and preparation in order to apply this technique to the field of electron solvation successfully. Standard methods of surface science such as thermal desorption spectroscopy (TDS) and scanning tunneling microscopy (STM) provide valuable information on the growth and the molecular structure of ice on Cu(111).[21]

The scheme of the experiment is given in Figure 1. An ultraviolet (UV) pump pulse (photon energy $h\nu_1$) excites electrons in the Cu substrate from below the Fermi energy (E_F) to bound intermediate states, where the excited electron can be transferred into the conduction band of the ice layer due to overlap of the wave functions. As shown in a previous communication, all the elementary steps can be separated on the basis of the 2PPE data.[22] Two different relaxation processes are observed: electrons transfer either back to the substrate, where they relax by electron−hole pair excitation, or they localize within 50 fs in the ice layer. The binding energy of the so-formed localized state increases with 270 meV/ps, a process which is attributed to electron solvation. These solvated electrons in front of the metal surface exhibit a finite lifetime of 0.1−1 ps and finally transfer back to the metal substrate. Moreover, a dependence of the electron solvation dynamics on the adlayer structure and coverage is observed.[21,22] Related 2PPE experiments were performed by Harris and co-workers, who studied localization of electrons in image potential states at alkane-covered Ag(111) surfaces by small polaron formation[19] and, more recently, solvation of localized electrons in polar molecular adlayers.[23,24]

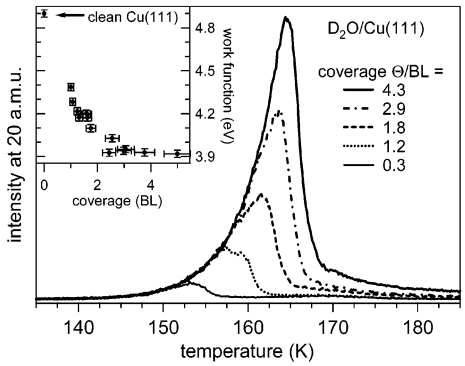

Figure 2. Thermal desorption spectra of D_2O/Cu(111) recorded at a heating rate of 1 K/s. The coverage is given in units of the mass equivalent of a single bilayer (BL) calibrated with respect to the TDS of D_2O/Ru(0001). The inset shows the work function obtained by 2PPE as a function of coverage.

It is the purpose of the present contribution to exploit the sensitivity of angle-resolved 2PPE on the electron momentum parallel to the surface and to extract information on the spatial extent of the solvated electron in ice layers on a metal substrate. These new results will be discussed in comparison to the present understanding of electron solvation dynamics in liquid water.

Sample Preparation and Experimental Details

The present experiment combines a surface science approach (i.e., adsorption of ultrathin ice layers on a Cu single-crystal surface prepared under ultrahigh vacuum conditions) with femtosecond time-resolved photoelectron spectroscopy. We describe first the sample preparation, which is important to achieve well-defined conditions.

Ultrathin layers of ice are grown on a single-crystal Cu(111) surface kept at 100 K in an UHV chamber (base pressure 1×10^{-10} mbar). The Cu substrate is prepared by cyclic Ar sputtering and annealing as described previously.[25] Neat deuterated water (99.9% purity) used for preparation of ice layers is purified further by freeze−pump−thaw cycles and dosed onto the sample surface by expansion through a pinhole from a reservoir with a pressure of 0.5 mbar into the vacuum chamber. A stainless steel tube guides the water vapor to the sample to minimize contamination of the UHV chamber. Only a minor pressure rise on the order of 1×10^{-10} mbar is observed during dosing. Deposition of water along the surface normal ensures the growth of nonporous amorphous ice layers as shown by

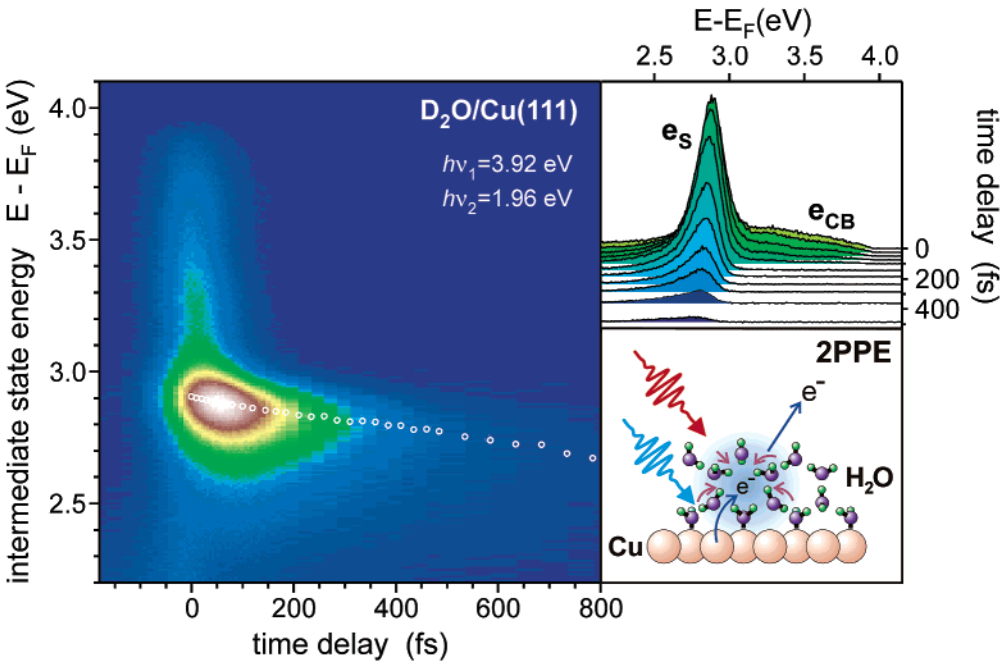

Figure 3. 2PPE intensity in a false color representation as a function of the pump−probe delay at different intermediate state energies $E - E_F$ measured for 4 BL D_2O/Cu(111) with $h\nu_1 = 3.90$ eV and $h\nu_2 = 1.95$ eV. The intermediate state energy scale is calculated by subtracting the probe photon energy $h\nu_2$ from the kinetic energy of the photoelectrons and adding the work function; open symbols represent the maximum intensity for different delays. The upper right panel shows data identical with that of time-dependent spectra; the data were taken at 100 K sample temperature. The lower panel represents an artist's view of the 2PPE experiment.

Kay and co-workers.[26] The adsorbed layers are characterized by thermal desorption (TD) spectroscopy, performed routinely after 2PPE measurements. A series of desorption spectra with increasing coverage of D_2O are given in Figure 2. We observe predominantly zero-order desorption kinetics, which indicates non-site-specific sublimation of ice, in agreement with earlier studies.[27] Integration of the TD spectra allows a relative determination of the coverage Θ, which was calibrated with respect to the TDS from the ordered and well-characterized $\sqrt{3} \times \sqrt{3}$ structure of D_2O/Ru(0001)[28] (denoted as one bilayer (1 BL) in the following).[29] At growth temperatures below 140 K water is known to adsorb in a metastable amorphous structure, which transforms into crystalline ice when the temperature exceeds 155 K.[27,30] The coverage dependence of the work function Φ, which denotes the energy difference between the Fermi energy E_F and the vacuum level E_{vac} (Figure 1), yields additional information on the growth mode of the adsorbed layer. Φ is measured by 2PPE directly (see below). As a function of coverage, the work function is substantially lowered from $\Phi = 4.9$ eV for clean Cu(111) upon adsorption of water (see inset of Figure 2). At a coverage of 3 BL the work function saturates at 3.95 eV, which suggests that ice adsorbs on Cu(111) initially not in a layer-by-layer growth mode. It rather takes about 3 BL before the Cu surface is completely covered by the adsorbate. At higher coverages (>3 BL), which is the range this paper is focused on, a smooth ice surface was observed by low-temperature STM.[21] The STM images reveal that the ice layer covers the Cu(111) surface completely and even follows monatomic steps of the substrate.

For time-resolved 2PPE experiments femtosecond laser pulses at 800 nm are regeneratively amplified at a repetition rate of 200 kHz in a commercial Ti:sapphire laser system.[25] The amplified pulses are fed into an optical parametric amplifier (OPA) to generate visible pulses, which are tunable within 1.7 and 2.7 eV. Frequency-doubled pulses $h\nu_1$ and the time-delayed visible fundamental $h\nu_2$ serve as pump and probe, respectively. The pulse duration of pump and probe is measured by their cross-correlation on the sample giving a full width at half-maximum below 100 fs. While the pump excites an electron from below the Fermi level to intermediate unoccupied states at energies $E - E_F = E_{kin} + \Phi - h\nu_2$, the probe pulse photoionizes the sample by lifting the electron above E_{vac} (Figure 1). Photoelectrons are detected in an electron time-of-flight spectrometer and analyzed according to their kinetic energy E_{kin} and momentum parallel to the surface $\hbar k_{||}$. Variation of the electron detection angle α with respect to the surface normal determines electron momentum according to

$$\hbar k_{||} = \sqrt{2 m_e E_{kin}} \cdot \sin \alpha \qquad (1)$$

where m_e denotes the free electron mass. $k_{||} = 0$ corresponds to electrons detected along the surface normal ($\alpha = 0$), while increasing α results in detection of electrons with nonzero $k_{||}$. For dispersion measurements the vacuum levels of sample and spectrometer have to be balanced due to their different work functions by applying a bias voltage to the sample. Thereby, deformation of the angular distribution of the emitted electrons by accelerating electric fields is minimized.

Results and Discussion

1. Electron Localization and Solvation Dynamics. Figure 3 details the temporal evolution of the 2PPE intensity for 4 BL D_2O/Cu(111) at intermediate state energies $E - E_F = 2.2-4.1$ eV. As the pump pulse alone causes an uncorrelated background signal of ~10% of the two-color spectra arising from 2PPE by two pump photons, this contribution is subtracted. The inset shows the identical data set depicted as 2PPE spectra at the indicated time delays Δt. Two features arising from photoexcitation of D_2O/Cu(111) are recognized: (i) a broad structureless continuum e_{CB} extending from 3.0 to 3.8 eV, which decays rapidly within the pulse duration, and (ii) a pronounced peak at 2.9 eV termed e_S. Its binding energy increases as a function of time delay by 270 meV/ps, which is determined

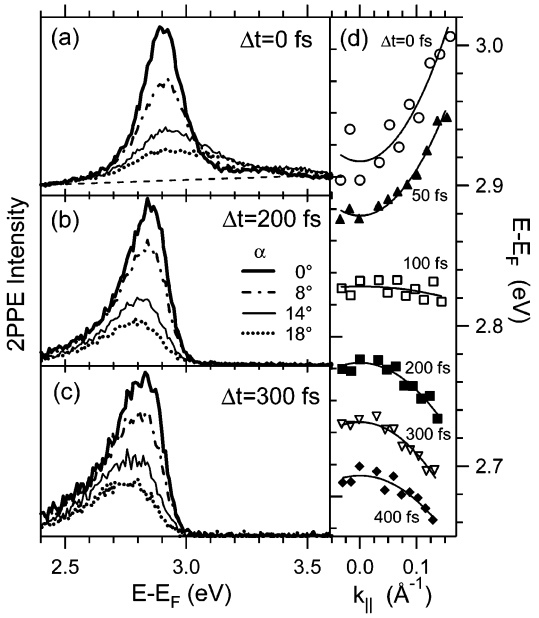

Figure 4. Angle-dependent 2PPE spectra of 3 BL D_2O/Cu(111) at zero delay (a), 200 fs (b), and 300 fs (c) normalized to intensity of the low energy cutoff at 0 fs; dispersion $E(k_{||})$ of the first moment of the electron intensity between 2.4 and 3.6 eV (d). In the case of $\Delta t \leq 100$ fs a linear background as indicated by the dashed line in (a) is subtracted to account for inelastically scattered electrons; solid lines in (d) are least-squares fits of parabolic functions to the data.

from an analysis of the time-dependent positions of the peak maxima (open symbols in Figure 3).

The pump pulse $h\nu_1 = 3.90$ eV excites electrons in the Cu substrate from below E_F to intermediate states below E_{vac}, as illustrated by Figure 1. Note that the photon energy of the pump pulse is much smaller than the band gap $E_{gap} = 8.2$ eV of ice.[31] Thus, direct photoexcitation in ice is unlikely and the broad continuum e_{CB} observed in Figure 3 is attributed to electrons which are transferred from the metal to the conduction band of ice. The transfer occurs due to the wave function overlap of the excited states in Cu and ice. In general, a nonequilibrium electron in the CB of ice can either relax within the band or can be transferred back to the metal. A different pathway for relaxation becomes available if localization of electrons is mediated by fluctuations of the electronic structure due to rearrangement of the molecular environment. Localization requires an energy E_{loc} in order to couple a certain width of energy levels within the conduction band to form a wave packet localized in space. However, E_{loc} may be exceeded by a stabilization energy E_{stab} due to the local reorganization of the molecular environment forming a potential well for the localized electron wave packet. As shown in ref 19 by Ge et al., the localization process may occur dynamically in two dimensions by formation of a small polaron. The energy of the localized state depends on a configuration coordinate that describes the molecular environment. Localization occurs only if a net gain ΔE_b in binding energy is achieved: $\Delta E_b = E_{stab} - E_{loc} > 0$.

Angle-resolved 2PPE allows determination of the localized or delocalized character of electronic states. The corresponding 2PPE spectra are given in Figure 4 for zero delay, $\Delta t = 200$ and 300 fs, and various emission angles. Two effects have to be considered. (i) Stabilization: Since the angle-dependent spectra are taken at different time delays, it is expected that the peak e_S at constant photoemission angle α shifts to lower energy due to electron solvation, as discussed above. (ii) Dispersion: At zero time delay the peak energy increases with α, which suggests a positive dispersion indicative for a delocalized state of the conduction band of ice. For longer delays the population of e_{CB} has decayed and the spectra are dominated by the peak e_S. The angle-dependent spectra (Figure 4b,c) show a decrease of the peak energy with increasing α. Since e_{CB} and e_S overlap partly at early times, we have analyzed the angle-dependent peak positions qualitatively by the first moment of the photoelectron distribution at $E - E_F = 2.4-3.6$ eV. Although e_{CB} has decayed for $\Delta t > 100$ fs (Figure 3), we have performed this analysis for all delays since it also regards the asymmetric line shape of e_S. The dispersion of the first moment along $k_{||}$ changes drastically as a function of time delay, as shown in Figure 4d. An initially positive dispersion turns into a constant one on the time scale of the pulse duration, which suggests a time-dependent transition from an initially delocalized state to a localized one: The initial Bloch-like state in the conduction band of ice turns into a wave packet with its spatial width Δx and the corresponding bandwidth in momentum $\Delta k_{||}$. In general, such a state is characterized by a constant dispersion, because a change in the wave vector within Δk addresses the same localized wave function. At larger delays we observe an apparently negative dispersion and one might infer that e_S is delocalized again. However, as we will show further below, this observation is consistent with a localized electronic state and includes information on the degree of localization of the solvated electron at the respective binding energy.

Turning back to the experimental data in Figure 3, one recognizes that the peak e_S merges with the low energy tail of e_{CB}. The population decay rates observed for e_{CB} and e_S are very different. While the e_{CB} decays within the duration of the laser pulse (<70 fs), e_S decays much slower in a nonexponential manner.[22] Even after 1 ps the solvated state, a few angstroms in front of the metal surface, remains populated. These observations suggest that a conduction band electron localizes at an energy close to the conduction band edge, comparable with electron localization through polaron formation.[19] The time scale of this localization process is below the temporal resolution of our experiment and is estimated to be on the order of 10 fs. Thus, we cannot decide to what extent the localization process occurs dynamically or in preexisting trapping sites such as defects or at uncompensated hydrogen bonds. For the subsequent electron solvation, which evolves on a picosecond time scale and is observed through the peak shift of e_S (Figure 3), the same question may be asked. Does the observed transient increase in binding energy originate from stabilization of the localized electron at a single site by molecular rearrangement, or does the localized electron subsequently gain binding energy by hopping between many different inhomogeneous distributed sites? We have therefore studied the temperature dependence of the solvation dynamics at 100 and 25 K. From the 2PPE data depicted in Figure 5, it is evident that the spectra do not change within this temperature interval. Since the mobility of electrons should depend on temperature, we exclude that the observed stabilization occurs due to hopping between different sites.

2. Analysis of Angle-Dependent 2PPE Spectra. To gain further insight into the nature of the localized electronic state e_S–attributed to solvated electrons in ice—we will discuss the temporal evolution of its dispersion and line shape in the following: A striking observation is the apparently negative dispersion of e_S after the conduction band contribution e_{CB} has decayed (see Figure 4). Since e_S and e_{CB} overlap partly, understanding and interpretation of their dynamics requires a separation of both features. Here a second observation becomes

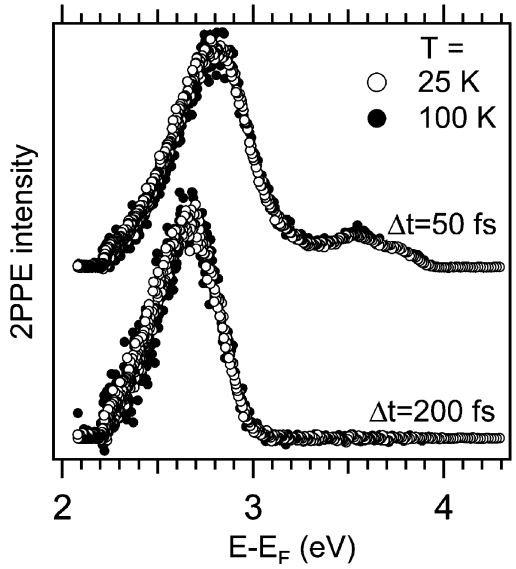

Figure 5. Time-resolved 2PPE spectra of 2 BL D_2O/Cu(111) at normal emission for 25 and 100 K. The spectra are normalized to the peak maximum and offset vertically for the two time delays.

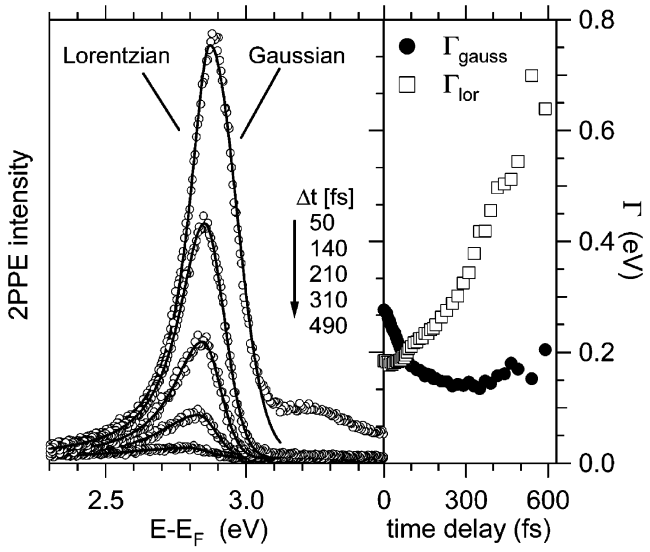

Figure 6. 2PPE spectra for D_2O/Cu(111) at the indicated time delays fitted by a Gauss (Lorentz) distribution on the high (low) energy side (left panel). The dependence of the half line widths Γ_{lor} and Γ_{gauss} on the time delay is depicted at the right.

important: As a function of time delay, the spectra show an increasing asymmetry (see inset of Figure 3), which has to be considered in the separation of e_S and e_{CB}. We, therefore, first analyze the temporal evolution of the line shape of e_S. The full spectra are fitted by an empirical function which consists of a Lorentz distribution on the low energy side of the peak and a Gauss distribution on the high energy side. As shown before for water clusters[32] and liquid water,[33] such an analysis reproduces the observed absorption and photoelectron spectra of hydrated electrons well. The left panel of Figure 6 depicts an exemplary set of spectra and least-squares fits. The line shape at time delays $\geq$140 fs are well reproduced, but at early delays the fit deviates from the experimental data above $\sim$3 eV due to the presence of e_{CB}. However, the peak shape of e_S is still well reproduced. In the right panel, the resulting line width is given as a function of Δt. The low energy line width Γ_{lor} increases continuously up to 3 times its initial value within 0.6 ps. The high energy part Γ_{gauss} varies only during early delays $\Delta t <$ 150 fs, when the conduction band contribution e_{CB} has not yet decayed and overlaps partly with e_S. Thus, the line width in this time interval does not represent only e_S but is influenced by e_{CB}. The exclusive contribution of e_S is found after e_{CB} has decayed ($\Delta t >$ 150 fs), where Γ_{gauss} is constant. The rather large half line width on the order of several 100 meV is attributed to an inhomogeneous distribution of localized electron states, which is caused by slight variations in the molecular environments of different solvation sites. With increasing degree of solvation the contribution of Γ_{lor} increases, which means that some electrons exhibit a faster increase in binding energy than the majority of solvated electrons represented by the peak maximum of e_S.

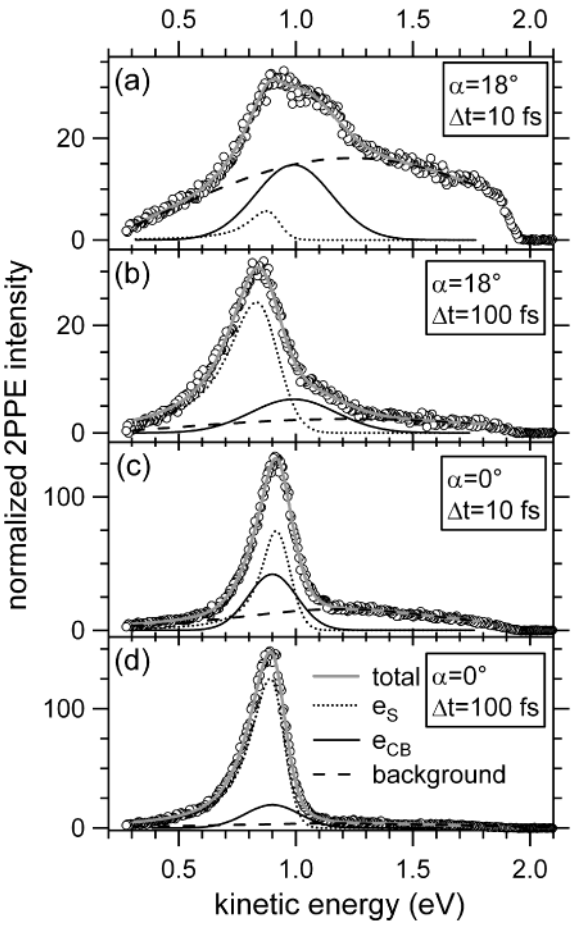

Figure 7. Decomposition of the 2PPE spectra into the contributions of conduction band (e_{CB}) (solid line) and of the solvated electron (e_S) (dotted line) by fitting the spectra with a two-contribution model, shown exemplarily for $\alpha = 18°$ and 0° and at $\Delta t = 10$ and 100 fs, respectively, in (a)−(d). A background due to scattered electrons is taken into account (dashed line); see text for details.

Now, we will come to a quantitative analysis of the angle-dependent spectra, to understand the pronounced change in the time-dependent dispersion, which is already visible by inspection of the first moment of the spectra displayed in Figure 4. A change from a positive to an apparently negative dispersion occurs on the time scale of 100 fs, i.e., parallel to the decay of the population in the conduction band. To separate these two contributions e_S and e_{CB}, we have fitted the angle-dependent data up to 400 fs with a two-peak model. The conduction band disperses with $k_{||}$ according to its effective electron mass. Its dispersion is assumed to be time-independent since it characterizes the unperturbed electronic structure of the adsorbate, and its spectral shape is considered to be described by a Gaussian distribution. The second contribution e_S at lower energy is

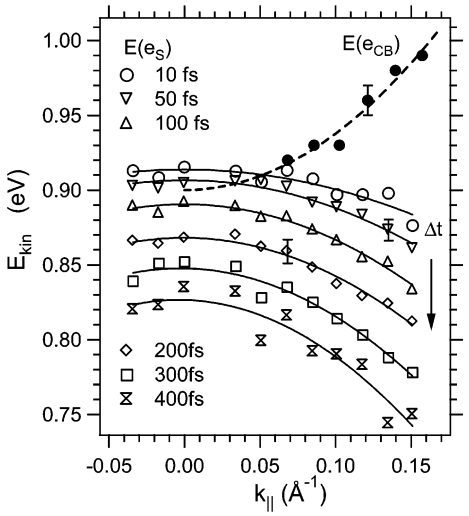

Figure 8. Dispersion of the conduction band and the solvated state in ice along $k_{||}$ determined from the two-peak model, as given in the text. The data points of the conduction band (●) are described by an effective electron mass equal to the free electron (dashed line). The peak maxima of the solvated state e_S are shown by open symbols up to $\Delta t = 400$ fs. Solid lines represent parabolic functions fitted to the data.

described by a Gaussian on the high energy side and by a Lorentzian at energies below the maximum, as introduced above.

At early delays, the spectra are superimposed on a considerable background, which is attributed to "hot" electrons in the metal and electrons scattered inelastically within the conduction band (dashed line in Figure 7). In the fitting procedure this background is described by a Gaussian with time-independent shape and an amplitude that decays with Δt. The sum of the three contributions fits the spectra at all delays and angles well, as depicted in Figure 7 by the gray solid line. At large angles and early delays one immediately recognizes the two peaks in the spectrum, as depicted in Figure 7a. The peak positions of e_S and e_{CB} resulting from that analysis are summarized in Figure 8. At small emission angles ($\alpha \leq 6°$) e_S and e_{CB} overlap and cannot be separated. To obtain the position of e_S at smaller angles, e_{CB} is fitted by a parabolic dispersion of a free electron gas with an effective mass of $1.0(2) \times m_e$ (with m_e being the free electron mass, dashed line in Figure 8). The binding energy of the conduction band minimum is then extrapolated from this fit for $\alpha \leq 6°$ to be 1.05 eV, i.e., 2.90 eV above E_F. Using these values for e_{CB}, the energy of e_S is determined by the same fitting procedure as for larger angles.

By this analysis it is found that e_{CB} exhibits a positive dispersion characteristic for delocalized states in the conduction band while e_S shows for all delays a decrease of binding energy with increasing $k_{||}$, a behavior which we denote as an apparently negative dispersion. At larger delays, when e_{CB} has decayed, the dispersion of the solvated electron contribution is measured exclusively. Thereby, it becomes clear that in the analysis of the first moment (Figure 4) the gradual transition from a positive to the apparently negative dispersion originates from the decay of the conduction band electrons e_{CB}.

In the following we will address the origin and the analysis of the apparently negative dispersion of the solvated electron peak. The energy of e_S changes by 30 meV comparing emission angles of 0° and 18° (Figure 4, Figure 8), which is about an order of magnitude smaller than the line width of e_S (Figure 6). According to eq 1, the photoelectron spectrum at a certain emission angle maps different values of $k_{||}$ depending on E_{kin}, as illustrated in the top panel in Figure 9. This effect becomes prominent in the observed angle-resolved 2PPE spectra of the

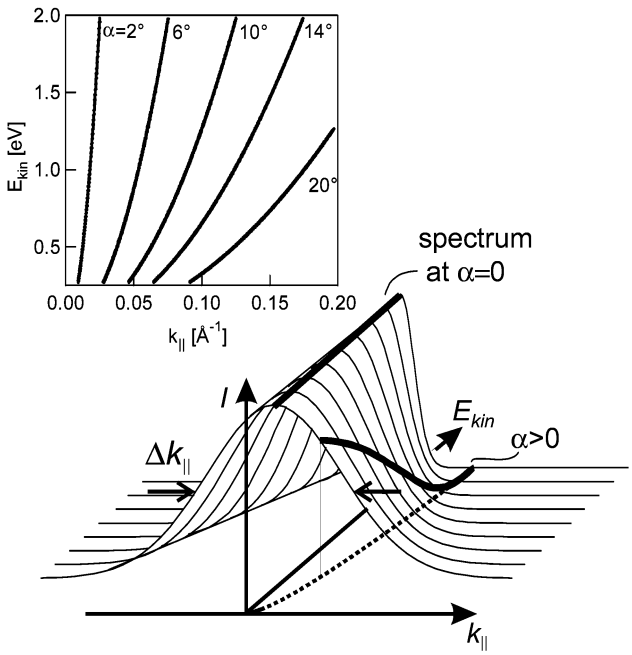

Figure 9. Illustration of the origin of the apparently negative dispersion of e_S. A broad constant spectrum at $\alpha = 0$ and E_{kin} of ~1 eV turns into a spectrum with increasing intensity at $\alpha > 0$ when E_{kin} is lowered (solid lines). As shown in the top panel, $k_{||}$ depends on the kinetic energy at a certain angle α according to eq 1. Therefore, a spectrum taken at constant α samples different $k_{||}$ values since the intensity distribution along $k_{||}$ is projected onto the plane described by E_{kin} and $k_{||}$ (dotted line). Due to the dispersion of $E_{kin}(k_{||})$, the intensity increases at $\alpha > 0$ if E_{kin} is lowered, even if the width $\Delta k_{||}$ is constant. For a negative slope $\partial(\Delta k_{||})/\partial E_{kin} < 0$—as plotted in the figure—this intensity increase is considerably enhanced.

state e_S due to the low kinetic energy of e_S (0.5−1.2 eV) and its broad line width. In the following, we discuss two different contributions to the apparently negative dispersion. (i) The first is variation of $k_{||}$ at a constant emission angle α for low kinetic energies below 1 eV (Figure 9, inset): We consider a localized electronic state with a finite spatial extent Δx in real space and a corresponding width $\Delta k_{||}$ in momentum space. For simplicity we assume for a moment that a constant 2PPE intensity would be observed over an extended energy interval at $\alpha = 0$. Then, any finite $\Delta k_{||}$ results in an intensity distribution $I(\alpha)$ at $\alpha > 0$, which rises for lower E_{kin} due to the variation of $E_{kin}(k_{||})$ at constant α (Figure 9, thick solid line above the dotted line). To achieve the real spectral shape of e_S, its spectral distribution has to be multiplied on top of the intensity distribution $I(\alpha)$ derived from $I(\alpha=0)$ and the resulting 2PPE intensity at $\alpha > 0$ will then still increase with decreasing E_{kin} within the line width. (ii) An increase in the width of the momentum distribution $\hbar\Delta k_{||}$ for decreasing E_{kin} with the slope $\partial(\Delta k_{||})/\partial E_{kin} < 0$ as plotted in Figure 9 leads qualitatively to the same phenomenon as (i). However, the broadening of $\Delta k_{||}$ for lower kinetic energy enhances the intensity increase.

Both scenarios are based on a localized electronic wave function with a finite width Δx in real space and $\Delta k_{||}$ in momentum space. To emphasize that a localized state is investigated although the observed dispersion is not constant, we term this behavior an apparently negative dispersion, which is, however, consistent with a localized state as discussed above.

3. Model Calculations. To identify the origin of the apparently negative dispersion from the two scenarios described above, we have performed model calculations. Naturally, the spatial extent of the solvated electron wave function, forming a wave packet by superposition of delocalized states, differs

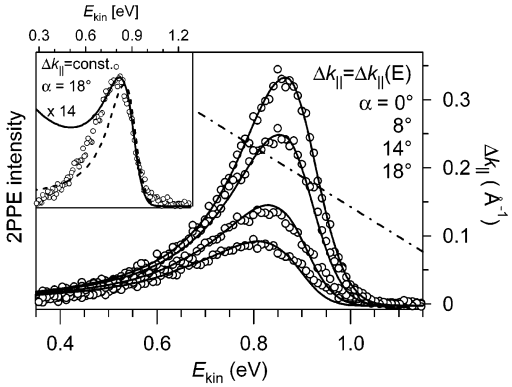

Figure 10. 2PPE intensity at 200 fs at the indicated angles (○) and model calculations (solid lines) that describe the data by taking into account an energy dependence $\Delta k_{||}(E)$ as given by the dash−dotted line. The solid lines are calculated from a least-squares fit to the spectrum at $\alpha = 0$. The inset shows the results for a constant $\Delta k_{||}$ of 0.20 Å^{-1} (dashed line) and 0.12 Å^{-1} (solid line, multiplied by 14), which both do not fit the data.

fundamentally from the size of a classical particle. However, in the present context we refer to the spatial extent of the solvated electron as the full width at half-maximum (fwhm) of the probability density. A localized state with the spatial extent $\Delta r = ((\Delta x)^2 + (\Delta y)^2 + (\Delta z)^2)^{1/2}$ (fwhm of the probability density) requires a momentum distribution $\hbar\Delta k = \hbar((\Delta k_x)^2 + (\Delta k_y)^2 + (\Delta k_z)^2)^{1/2}$. Here z is the direction along the surface normal. In photoemission from ordered surfaces with translation symmetry, the parallel component of the electron momentum is conserved, while the component along the surface normal k_z is changed by the potential barrier at the surface between Bloch states in the substrate and the vacuum continuum. Therefore, the information of the experiment is restricted to $\Delta k_{||}$ and Δx, where rotational symmetry is assumed in the surface plane ($\Delta k_x = \Delta k_y = \Delta k_{||}$; $\Delta x = \Delta y$). An analysis of the angular dependence of the spectral intensity requires normalization of the angle-dependent 2PPE spectra, which considers angle-dependent changes of the detection probability. Because it is not feasible to determine all changes in the excitation rate, analyzer transmission, or influence of small stray fields, we use a different approach. All angle-dependent 2PPE spectra are normalized to their low energy intensity at zero delay. These secondary electrons originate from photoexcited hot electrons in the Cu substrate, which scatter inelastically.[34] The corresponding femtosecond electron dynamics have been studied extensively on metal surfaces.[35]

To analyze the angle-dependent spectra in further detail and to extract information about Δx, we assume that the 2PPE intensity of the state e_S is distributed along $k_{||}$ according to a Gaussian $I(k_{||})$ with a width $\Delta k_{||}$. To describe the 2PPE data at $\alpha > 0$, the measured 2PPE spectrum at $\alpha = 0$ is weighted by that $\Delta k_{||}$ distribution $I(k_{||})$. Several dependencies of $\Delta k_{||}$ on energy were used, as shown exemplarily in Figure 10. We have first tried to model the data under the simple assumption that $\Delta k_{||}(E)$ = constant, i.e., for a fixed width Δx of the localized state. As seen from the inset of Figure 10, the spectra are not reproduced under this constraint. For $\Delta k_{||} = 0.20$ Å^{-1} the intensity agrees roughly with the 2PPE data but the spectral shape is not obtained. A smaller value $\Delta k_{||} = 0.12$ Å^{-1} yields at higher energy a better spectral shape but provides too little intensity (shown scaled ×14). Moreover, the intensity on the low energy side deviates strongly from the data. However, if we consider a $\Delta k_{||}(E)$ increasing linearly with decreasing energy as shown by the dash−dotted line in Figure 10 (main panel), the angle-dependent 2PPE spectra are reproduced very well. Our model calculations show that the width of the electron momentum $\Delta k_{||}$ increases with the binding energy of the solvated electron, i.e., with increasing degree of solvation. Thus, the angle-resolved 2PPE data contain information on the electron solvation process complementary to the energetic stabilization dynamics. We conclude that the degree of spatial constriction of the solvated, localized electron increases simultaneously with the energetic stabilization dynamics. In other words, an electronic wave function increases its binding energy in a given potential if the electron's spatial extent is decreased.

The question arises of how far an absolute value for the spatial extent of the solvated electron wave function can be obtained from angle-resolved 2PPE data. As referred to above, $\Delta k_{||}$ corresponds to the spatial extent Δx and Δy of the solvated electron in the surface plane. However, $k_{||}$ is not a good quantum number, as the translational symmetry is broken for a localized state. By leaving the potential well of the solvated electron $V_S(x,y,z)$, the photoemitted electron changes not only its perpendicular momentum component, but also the parallel one, which is thus not conserved. As depicted in Figure 11, V_S presents a potential well at $x = 0$ and $z = z_0$ and approaches the limit of the unperturbed molecular continuum for large x and z. Strictly speaking, the initial value of $k_{||}$ inside the potential well is not accessible by angle-dependent measurements. However, 2PPE measures not only the electron momentum but also the binding energy of the solvated electron and the conduction band depicted as levels E_S and E_{CB} in Figure 11. Thus, the height of the lateral potential barrier, which the solvated electron has to overcome in order to leave V_S, can be estimated. To account for the change of the electron momentum of the solvated electron photoemitted from the bound state in V_S, the energy difference $E_{CB} - E_S$ has to be considered. This leads to a small correction $\gamma = \sqrt{(E-E_S)/E}$ of the electron momentum determined from the angle-dependent spectra, according to $\hbar k_{||} = \gamma \sin\alpha\sqrt{2m_eE}$, where E is the electron energy above the bottom of the conduction band inside the adlayer.

To discuss the magnitude of the correction γ, we use typical values observed in our experiment. With E_{vac} located about 1 eV above E_{CB}, $E_{kin} = 0.8$ eV, and $E_S(\Delta t{=}200\text{ fs}) = -75$ meV, we find $\gamma = 1.02$. Even at the maximum delay of 1.5 ps with $E_S(1.5\text{ ps}) = -300$ meV, γ amounts to only 1.08. That means an electron momentum $k_{||} = 0.100$ Å^{-1} experimentally determined at $\Delta t = 200$ fs has to be corrected to 0.102 Å^{-1} to account for the change of electron momentum by leaving V_S in a direction parallel to the surface. Since the correction is on the order of a few percent, we conclude that the 2PPE experiment in fact provides a fairly good absolute measurement of $\Delta k_{||}$ within the limits discussed above.

It is thus tempting to interpret the Fourier transformation of $\Delta k_{||}$ as the size Δx of the solvated electron, as introduced by Harris and co-workers.[23] In our work on electron solvation in ice layers, Δx obtained by Fourier transformation is found to depend on the kinetic energy and changes from 19 Å at E_{kin} = 1 eV to 9 Å at 0.64 eV, respectively. As we point out in the following, the relation between $\Delta k_{||}$ and the size of the solvated electron may not be governed solely by a Fourier transformation, because final state effects in the photoemission process might contribute as well.[37] We have constructed a simple potential depicted in Figure 11 to illustrate this effect. The solvated electron is bound in front of the Cu surface in a potential well $V_S(x,z)$ as a function of two coordinates: the lateral dimension x (assuming rotational symmetry) and the direction z along the

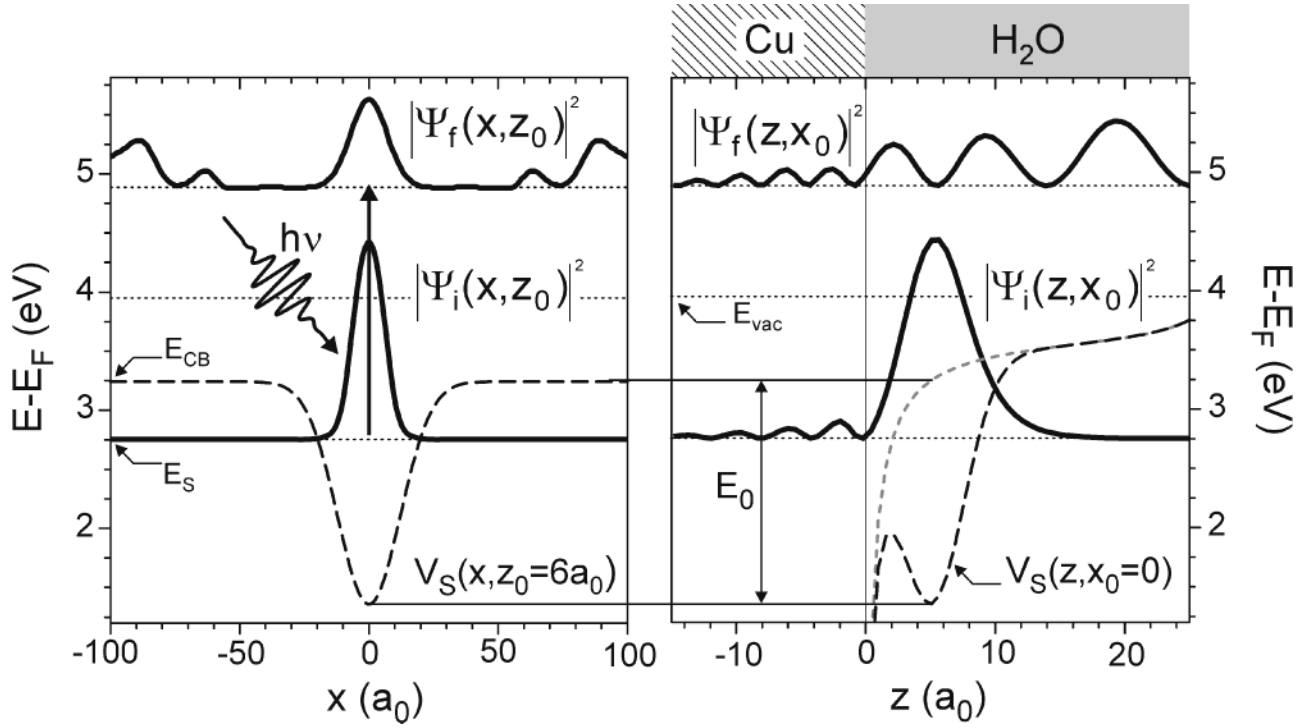

Figure 11. One-dimensional representation of the two-dimensional potential of the solvated electron in the ice layers adsorbed on Cu(111). In the lateral dimension (left panel) the potential V is shown along x at $z_0 = 6a_0$, where the potential minimum occurs. For the y direction rotational symmetry is assumed in the surface plane. Along the surface normal, the image potential in ice (gray dashed line) and the potential of the solvated electron add up to $V(z,x_0)$. Two-dimensional wave functions are calculated from V_S: Ψ_i, which is bound to the potential of the solvated electron, and the final state Ψ_f above the vacuum level. For the latter one state out of a continuum of states is depicted.[36]

surface normal. V_S consists of two contributions: (i) The image potential in front of the metal surface along z, where we use the potential derived by Chulkov et al.[38] modified by the dielectric continuum of the unperturbed ice layer in front of the surface. For a detailed description of the dielectric continuum model, see ref 39. (ii) For simplicity, the solvated electron potential is modeled by a Gaussian with different widths along x and z (parallel 5 times broader than perpendicular to the surface). The two-dimensional potential $V_S(x,z)$ is taken as the sum of the solvated electron potential along x and z and the image potential along z. Two-dimensional wave functions were calculated for the bound (i.e., solvated electron) state and final states at energies according to the photon energies used in the experiment. The initial and final state wave functions $|\Psi_i(x,z)|^2$ and $|\Psi_f(x,z)|^2$are plotted in Figure 11 for two one-dimensional cuts along x, $z_0 = 6a_0$ (left panel) and z, $x_0 = 0$ (right panel), where a_0 is the Bohr radius. Although $\Psi_f(x,z_0)$ is delocalized laterally, it is strongly modified compared to the wave function of a free electron.

The above considerations show that the deviation of the final state $\Psi_f(x,z)$ from free electron behavior parallel to the surface is also confined in the same spatial region as the initial state $\Psi_i(x,z)$, although to a different extent. Both wave functions are characterized by their spread in momentum, which both contribute to the measured angular dependence of the 2PPE intensity. The question if angle-resolved 2PPE allows an absolute measurement of the size of the solvated electron implies understanding which of these two contributions—the initial or the final state—dominates the experimentally observed angle-dependent photoelectron intensity. Since the 2PPE intensity is determined by the energy and momentum dependence of the transition matrix elements, this question calls for further theoretical investigations, which are currently underway.

4. Discussion and Comparison with Literature. Due to the broad literature base on the electron solvation dynamics in liquid water, it is interesting to compare the dynamics of the liquid and solid phase with the present results at the ice/metal interface. Considering the dielectric relaxation rate in thermal equilibrium as a characteristic response time of the medium which determines the solvation dynamics, one would expect a much slower dynamics for ice compared to the liquid as the dielectric relaxation in ice takes at 185 K about a millisecond compared to nano- and picoseconds in liquid water.[40] However, this estimate is at variance with the fact that the generation of solvated electrons is a nonequilibrium process. As we will point out, the energetic stabilization rates for electron solvation differ by less than an order of magnitude for ice and the liquid, which we attribute to the considerable energy gain associated with electron solvation. This energy is dissipated by the molecular environment, which may increase the solvent's mobility and may serve as an explanation for the ultrafast time scale of electron solvation dynamics in ice.

We start out by discussing the *spectral features*. Various time-resolved optical absorption studies of the formation of solvated electrons in neat liquid water agree on the observation of a sequence of spectral signatures: (i) Immediately after generation of excess electrons, early precursors to the solvated electron have been identified recently by transient mid-IR spectroscopy.[7,41] These species exhibit characteristic spectral features in the mid-IR ($\lambda > 1.5$ μm), which depend in a complex way on the details of the generation process (e.g., multiphoton excitation of water or photoejection from ferrocyanide).[7,41] Note that the "surface science" approach used in this work circumvents this complication as water is not optically excited but electrons are injected from the metal substrate by photoinduced electron transfer across the ice−Cu interface. (ii) Subsequently, within 100−200 fs a "weakly bound" species e_{wb} (often attributed as the "presolvated" or "wet" electron) is formed, with an optical absorption extending into the near-IR.[3,7,33,42] The origin of e_{wb} is under discussion: several explanations such as

the p-state in the cavity model, an intermediate, excited state of water H_2O^*, and other precursors have been considered. (iii) Finally, after decay of e_{wb} with time constant of typically 500 fs a "strongly bound" species e_{sb} is formed, which absorbs in the visible. Its absorption spectrum at long times is identical to that of the fully hydrated electron.

In the static optical absorption spectra of solvated electrons in ice, basically the same two features (e_{wb} and e_{sb}) are observed at slightly different wavelengths.[43] However, time-resolved studies of the initial electron solvation dynamics in bulk ice are not available. As in our present work on thin ice layers on a metal surface the time-resolved 2PPE spectra are also characterized by two features, e_{CB} and e_S, it is tempting to compare these features to the ones observed by optical absorption spectra of solvated electrons in liquid water. Although, e_{wb} and e_{sb} in liquid water exhibit a fast and slow relaxation as found for e_{CB} and e_S in the D_2O/Cu system, the dynamics of the corresponding processes are quite different. In particular, e_{CB} observed for D_2O/Cu relaxes extremely fast (within the pulse duration) and, moreover, exhibits the characteristic dispersion of delocalized electrons. It is therefore attributed to excess electrons in the conduction band.

The major signature of electron solvation in D_2O/Cu(111) is the time-dependent stabilization of e_S, which might correspond to the "strongly bound" species e_{sb} for liquid water. In both cases, stabilization of the solvated electron by a few hundred millielectronvolts is observed within several picoseconds.[16,33,44] While in the transient absorption spectra of the liquid the peak energy depends exponentially on the time delay up to about 3 ps, we observe a quasi-linear dependence within the first picoseconds. This finding is most probably related to the energy window probed in our experiment, which is rather small compared to the total stabilization, because the peak shifts out of the probed energy interval before 2 ps. We expect that at long delays the binding energy of the solvated electron will reach an asymptotic level at energies below the low energy cutoff.

On the basis of the present 2PPE data we do not observe any precursor to the solvated electron other than e_{CB}, which is in contrast to Laenen et al., who have resolved various precursors attributed to localized electrons in the liquid.[7] We believe that these differences in the early time dynamics originate from the different generation processes of the excess electrons. Supposing that the relaxation dynamics in ice layers on a metal do not differ fundamentally from the one in neat liquid water, our data would thus support the interpretation of relaxation in a hot ground state suggested by Unterrainer et al.[11] and Vilchiz et al.[44] However, as electronic relaxation at metals occurs on the few femtoseconds time scale and an efficient injection mechanism is required to transfer electrons into the ice, the strong coupling to the metal substrate might rapidly damp excited-state dynamics in the ice/Cu system. This would hinder the observation of an excited-state precursor at the ice/metal interface, although such species might exist in the liquid.

Next, we discuss briefly *line shapes*: As shown above, the 2PPE spectra of the feature e_S are described well by the same empirical form, which fits the solvated electron absorption spectra, if the 2PPE spectra are plotted as a function of binding energy.[45] Pépin et al. have performed an analysis of the half spectral widths on the high and low energy sides of e_{sb} during the electron solvation process[33] (compare to Figure 6). While these authors find a constant Lorentzian width (low electron energy side in 2PPE, high photon energy side in absorption spectroscopy), the Gaussian width (high electron energy side in 2PPE, low photon energy side in absorption spectroscopy) decreases exponentially as a function of time delay from 0.5 eV at 0.8 ps to 0.35 eV at 3 ps. However, e_{sb} overlaps with e_{wb}, which might mask the behavior of e_{sb}. This complication is also addressed in the present analysis. The corresponding result for 2PPE (Figure 6) is limited to $\Delta t < 600$ fs and differs significantly in the temporal evolution. We find a constant Gaussian and an increasing Lorentzian line width, which is attributed to inhomogeneous broadening. Unfortunately, the time scales of the two experiments do not overlap well, which makes further discussion difficult. However, the qualitative similarity of the spectral shape is remarkable.

Summarizing the comparison with the liquid, we point out that the time scale of electron *stabilization* in ice is comparable to that in the liquid, rather than evolving much slower as the dielectric relaxation rate in thermal equilibrium would suggest. Moreover, the *formation* of solvated electrons observed in the feature e_S in ice/Cu occurs within 50 fs, which is considerably faster than the appearance of the strongly bound electron in the liquid. Note also that the spectral shape observed for the solvated species can be described by the same empirical function used for the absorption spectra of the liquid and clusters.

Finally, we discuss a related experiment studying electron solvation in a molecular layer on a metal substrate. The work of Miller et al.[23,24] addresses questions closely related to the present study by measuring the electron solvation dynamics with 2PPE for polar molecules adsorbed on Ag(111). These authors observe for a coverage of a single monolayer a time-dependent stabilization of the image potential states, which are known to be delocalized in front of the surface. Consequently, it is suggested that the stabilization occurs due to collective reorientation of the dipoles, where the molecules keep their parallel alignment over a diameter given by the coherence length of the electron in the image potential state. The question arises of how many molecules can be reoriented by stabilizing a single electron, which presents an independent estimation of the size of the stabilized electron. Assuming that the stabilization potential of each individual molecule requires a depth along the rearrangement coordinate of more than $3kT$ and considering equality of gain in electronic binding energy and energy required for the total molecular reorganization, the observed stabilization energy of 280 meV at 90 K results in 30−40 molecules, which can take part in the electron-induced rearrangement. However, this suggests that the electron is localized on a patch consisting of less than 40 molecules. To understand and to relate these very interesting results of Harris and co-workers with the solvation dynamics observed in ice, the required lateral size for the formation of a delocalized image potential state must be known. However, a determination of the coherence length is difficult due to inhomogeneous broadening.

Conclusion

Time- and angle-resolved two-photon-photoelectron spectroscopy has been used to identify the elementary steps of electron solvation in ice layers on Cu(111). These are (i) photoinduced electron transfer into the conduction band of ice, (ii) localization of the electronic Bloch state followed by molecular reorientation of the water dipoles leading to (iii) energetic stabilization and solvation of the electron, and (iv) back transfer of the excited electron to the metal substrate due to residual wave function overlap. The 2PPE spectra of ice layers on Cu(111) are characterized by two spectral features. A broad continuum in the range of the ice conduction band decays within the pulse duration below 70 fs. It corresponds with the IR

absorption observed in time-resolved optical spectroscopy of liquid water and ice, but lacks the complication of precursors due to photoionization of the water molecule since in the present study the electron is injected from the metal substrate. Evidence for electron solvation is found in the 2PPE study by stabilization of a localized species e_S, characterized by dispersion measurements at different delays. A binding energy that increases with time due to electron stabilization achieved by molecular rearrangement is observed for this state. A detailed analysis of the temporal evolution of the dispersion, which involves separation of the overlapping conduction band and solvated electron contribution, results in an apparently negative dispersion of the localized state. This feature is characteristic for a distribution of solvated species caused by the rather large inhomogeneous line width of several 100 meV and contains information on the width of the parallel electron momentum distribution $\hbar\Delta k_{||}$, which is required to form the localized and solvated state. $\Delta k_{||}$ is found to increase with increasing binding energy. On the basis of this experimental result, we conclude that an increasing degree of solvation requires coupling of more bandwidth of $k_{||}$, corresponding to an increase in constriction of the solvated electron wave function. The spatial extent of the electronic wave function resulting from $\Delta k_{||}$ is on the order of 10−20 Å, depending on the electronic kinetic energy. However, this result may be influenced by the final electronic state which deviates from free electron states due to the perturbation by the potential well of the solvated electron and therefore does not exclusively represent the spatial extent of the solvated electron localized in its bound state.

Our experimental approach might be promising to develop further understanding of electron solvation dynamics in water by reducing the number of involved elementary processes and thereby concentrate on the interaction of excess electrons with a polar molecular environment.

Acknowledgment. We thank T. Klamroth and P. Saalfrank for providing the solvated electron wave functions, K. Horn for fruitful discussions, and G. Ertl for supporting the experiments at the Fritz-Haber-Institut der MPG. We acknowledge financial support by the Deutsche Forschungsgemeinschaft through SPP 1093.

References and Notes

(1) Barnett, R. N.; Landman, U.; Nitzan, A. *Phys. Rev. Lett*. **1989**, *62*, 106.
(2) Weber, J. M.; Kim, J.; Woronowicz, E. A.; Weddle, G. H.; Becker, I.; Cheshnovsky, O.; Johnson, M. A. *Chem. Phys. Lett.* **2001**, *339*, 337.
(3) Migus, A.; Gauduel, Y.; Martin, J. L.; Antonetti, A. *Phys. Rev. Lett*. **1987**, *58*, 1559.
(4) Long, F. H.; Lu, H.; Eisenthal, K. B. *Phys. Rev. Lett*. **1990**, *64*, 1469.
(5) Silva, C.; Walhout, P. K.; Yokoyama, K.; Barbara, P. F. *Phys. Rev. Lett*. **1998**, *1086*, 80.
(6) Emde, M. F.; Baltuska, A.; Kummrow, A.; Pshenichnikov, M. S.; Wiersma, D. A. *Phys. Rev. Lett*. **1998**, *80*, 4645.
(7) Laenen, R.; Roth, T.; Lauberau, A. *Phys. Rev. Lett*. **2000**, *85*, 50.
(8) Schnitker, J.; Motakabbir, K.; Rossky, P. J. *Phys. Rev. Lett*. **1988**, *60*, 456.
(9) Prezhdo, O. V.; Rossky, P. J. *J. Phys. Chem.* **1996**, *100*, 17094.
(10) Yang, C.-Y.; Wong, K. F.; Skaf, M. S.; Rossky, P. J. *J. Chem. Phys.* **2001**, *114*, 3598.
(11) Hertwig, A.; Hippler, H.; Unterreiner, A.-N. *Phys. Chem. Chem. Phys*. **2002**, *4*, 4412.
(12) Lehr, L.; Zanni, M. T.; Frischkorn, C.; Weinkauf, R.; Neumark, D. M. *Science* **1999**, *284*, 635.
(13) Kevan, L. *Acc. Chem. Res.* **1981**, *14*, 138.
(14) Son, D. H.; Kambhampati, P.; Kee, T. W.; Barbara, P. F. *Chem. Phys. Lett*. **2001**, *342*, 571.
(15) Son, D. H.; Kambhampati, P.; Kee, T. W.; Barbara, P. F. *J. Phys. Chem. A* **2001**, *105*, 8269.
(16) Kambhampati, P.; Son, D. H.; Kee, T. W.; Barbara, P. F. *J. Phys. Chem. A* **2002**, *106*, 2374.
(17) Höfer, U.; Shumay, I. L.; Reuss, Ch.; Thomann, U.; Wallauer, W.; Fauster, Th. *Science* **1997**, *277*, 1480.
(18) Roth, M.; Pickel, M.; Wang, J.; Weinelt, M.; Fauster, Th. *Phys. Rev. Lett*. **2002**, *88*, 096802.
(19) Ge, N.-H.; Wong, C. M.; Lingle, R. L., Jr.; McNeill, J. D.; Gaffney, K. J.; Harris, C. B. *Science* **1998**, *279*, 202.
(20) Marinica, D. C.; Ramseyer, C.; Borisov, A. G.; Teillet-Billy, D.; Gauyacq, J. P.; Berthold, W.; Feulner, P.; Höfer, U. *Phys. Rev. Lett*. **2002**, *89*, 046802.
(21) Gahl, C.; Bovensiepen, U.; Frischkorn, C.; Morgenstern, K.; Rieder, K.-H.; Wolf, M. *Surf. Sci*. **2003**, *108*, 532−535.
(22) Gahl, C.; Bovensiepen, U.; Frischkorn, C.; Wolf, M. *Phys. Rev. Lett*. **2002**, *89*, 107402.
(23) Miller, A. D.; Bezel, I.; Gaffney, K. J.; Garrett-Roe, S.; Liu, S. H.; Szymanski, P.; Harris, C. B. *Science* **2002**, *297*, 1163.
(24) Liu, S. H.; Miller, A. D.; Gaffney, K. J.; Szymanski, P.; Garrett-Roe, S.; Bezel, I.; Harris, C. B. *J. Phys. Chem. B* **2002**, *106*, 12908.
(25) Knoesel, E.; Hotzel, A.; Wolf, M. *Phys. Rev. B* **1998**, *57*, 12812.
(26) Stevenson, K. P.; Kimmel, G. A.; Dohnálek, Z.; Smith, R. S.; Kay, B. D. *Science* **1999**, *283*, 1505.
(27) Hinch, B. J.; Dubois, L. H. *J. Chem. Phys*. **1992**, *96*, 3262.
(28) Held, G.; Menzel, D. *Surf. Sci*. **1995**, *327*, 301.
(29) The term "bilayer" refers to the puckered structure of bulk ice.
(30) Smith, R. S.; Kay, B. D. *Nature* **1999**, *398*, 788.
(31) Shibaguchi, T.; Onuki, H.; Onaka, R. *J. Phys. Soc. Jpn*. **1977**, *42*, 152; E_{gap} taken at 50% threshold.
(32) Coe, J. C. *Int. Rev. Phys. Chem*. **2001**, *20*, 33.
(33) Pépin, C.; Goulet, T.; Houde, D.; Jay-Gerin, J.-P. *J. Phys. Chem. A* **1997**, *101*, 4351.
(34) The hot electrons occur in the center of the orientational band gap of Cu(111) at 2.5 eV, and within the used angles we can safely rely on a constant hot electron background. Thus, normalization of the angle-dependent spectra of e_S to the low energy background takes into account changes of the detection probability.
(35) Petek, H.; Ogawa, S. *Prog. Surf. Sci*. **1997**, *56*, 239.
(36) To match the experimentally observed energy levels, a dielectric constant of 3 and an electron affinity of 0.3 eV were used for the dielectric continuum model.
(37) In ref 23 a conservation of $k_{||}$ was assumed and deviations of the final state from free electron behavior parallel to the surface were neglected.
(38) Chulkov, E. V.; Silkin, V. M.; Echenique, P. M. *Surf. Sci*. **1999**, *437*, 330.
(39) McNeil, J. D.; Lingle, R. L.; Jordan, R. E.; Padowitz, D. F.; Harris, C. B. *J. Chem. Phys.* **1996**, *105*, 3883. Hotzel, A. Ph.D. Thesis. Freie Universität Berlin, 1999, chapter 4; http://www.diss.fu-berlin.de/1999/55/indexe.html.
(40) Bergman, R.; Swenson, J. *Nature* **2000**, *403*, 283.
(41) Anderson, N. A.; Hang, K.; Asbury, J. B.; Lian, T. *Chem. Phys. Lett*. **2000**, *329*, 386.
(42) Hertwig, A.; Hippler, H.; Unterrainer, A. N. *J. Phys.: Condens. Matter A* **2000**, *12*, 165.
(43) Gillis, H. A.; Quickenden, T. I. *Can. J. Chem*. **2001**, 79, 80.
(44) Vilchiz, V. H.; Kloepfer, J. A.; Germaine, A. C.; Lenchenkov, V. A.; Bradforth, S. E. *J. Phys. Chem. A* **2001**, *105*, 1711.
(45) If $E - E_F$ or the kinetic energy is used, the axis has to be multiplied by −1, because a lower electron energy requires a higher photon energy to photoexcite the solvated electron into CB or the continuum and vice versa.